

PAPER

Integrative Analysis and Imputation of Multiple Data Streams via Deep Gaussian Processes

Ali A. Septiandri^{1,*}, Deyu Ming², F. A. Diaz De la O³, Takoua Jendoubi¹
and Samiran Ray⁴

¹Department of Statistical science, University College London, London WC1E 7HB, UK, ²School of Management, University College London, London WC1E 6BT, UK, ³Clinical Operational Research Unit, University College London, London WC1H 0BT, UK and

⁴Paediatric Intensive Care Unit, Great Ormond Street Hospital For Children NHS Foundation Trust, London WC1N 3BH, UK

*Corresponding author. ali.septiandri.21@ucl.ac.uk

FOR PUBLISHER ONLY Received on Date Month Year; revised on Date Month Year; accepted on Date Month Year

Abstract

Motivation: Healthcare data, particularly in critical care settings, presents three key challenges for analysis. First, physiological measurements come from different sources but are inherently related. Yet, traditional methods often treat each measurement type independently, losing valuable information about their relationships. Second, clinical measurements are collected at irregular intervals, and these sampling times can carry clinical meaning. Finally, the prevalence of missing values. Whilst several imputation methods exist to tackle this common problem, they often fail to address the temporal nature of the data or provide estimates of uncertainty in their predictions.

Results: We propose using deep Gaussian process emulation with stochastic imputation, a methodology initially conceived to deal with computationally expensive models and uncertainty quantification, to solve the problem of handling missing values that naturally occur in critical care data. This method leverages longitudinal and cross-sectional information and provides uncertainty estimation for the imputed values. Our evaluation of a clinical dataset shows that the proposed method performs better than conventional methods, such as multiple imputations with chained equations (MICE), last-known value imputation, and individually fitted Gaussian Processes (GPs).

Availability and implementation: The source code of the experiments is freely available at: <https://github.com/aliakbars/dgpsi-picu>.

Contact: ali.septiandri.21@ucl.ac.uk

Key words: critical care medicine, deep Gaussian process, missing data, stochastic imputation

1. Introduction

One of the main challenges in analysing healthcare data is that they are usually collected from multiple measurement streams. A patient's medical record may include data from different sources, such as medical histories, laboratory tests, and imaging studies [21]. Integrating and analysing the data can thus be challenging, as the various data sources may use different formats, units, and scales. For example, a patient's CO₂ level may be measured breath by breath directly from a ventilator circuit, but their albumin levels are measured daily from blood sample tests. Thus, aligning these multiple streams will result in missing values. Simply removing missing values and performing a complete case analysis would not suffice, since useful observations might be lost [53].

Another challenge of working with healthcare data is that it is often irregularly and informatively sampled [15]. The irregularity refers to the data collection at different times and intervals due to the sample sources. Additionally, there is the problem of informative sampling, where one

might observe an extended period of intervals because the patient is getting better, making the clinicians reduce the frequency of monitoring [9]. These circumstances make it challenging to assess a patient's health and make informed decisions accurately. As the sampling frequency is, by nature, informative, it will be more difficult to detect subtle changes in unobserved variables retrospectively.

Current practices for handling missing values in healthcare data often prioritise simplicity over complexity. A common approach is using the last-known value imputation, also known as the last-observation-carried-forward (LOCF) method, which fills in missing values by extending the most recent available measurement for a specified time period [45]. While this method is straightforward, it overlooks the correlation between covariates. On the other hand, multiple imputation by chained equations (MICE), another commonly widely used method, uses cross-sectional information between covariates but treats each observation independently [40, 51].

More recently, deep neural networks have become increasingly popular for handling missing values in healthcare data [30, 9, 8, 55]. However, these methods have a limitation: they typically do not provide estimates of uncertainty in their predictions. This can be a problem in healthcare data analysis, where medical observations and interpretations inherently contain uncertainty, which may come from measurement error, inherent noise in the signal, or the use of surrogate markers. When this uncertainty in the input data is not accounted for, it can lead to unreliable model predictions [7].

This study aims to tackle the problem of handling missing values in multivariate time series data by leveraging both longitudinal and cross-sectional information. We use a deep Gaussian process (GP) model with stochastic imputation [33, 34] where time is the input to predict the target variable through covariates in the model's latent layer. By fitting the model jointly, the available information can be used as leverage to impute missing values stochastically. Moreover, this method comes with uncertainty estimation. This approach is evaluated against a baseline method that fits individual GPs to covariates using complete case analysis for model training and subsequent imputation.

A deep Gaussian process model is a hierarchical structure of GP nodes organised in layers to represent latent variables [11]. Each node receives input from the previous layer and produces output that serves as input for the next layer. The observed data points appear at the final layer of this hierarchy. While single-layer GP models are limited by the kernel function used, which can be highly parameterised to learn complex data patterns, a deep GP model learns them non-parametrically via the hierarchy, thus having fewer hyperparameters to optimise [41]. Due to their ability to provide uncertainty estimates, deep GP models have applications in real-life domains, including aero-propulsion system simulation [6], crop yield prediction from remote sensing data [56], and uncertainty estimation in electronic health records [29].

The remainder of the paper is structured as follows. The clinical problem that motivated this research is explained in Section 2. GPs and deep GPs are reviewed in Section 3, where the methodological approach and alternative techniques for handling missing values in multivariate time series data are described. The proposed deep GP using stochastic imputation is validated by applying it to a clinical case study in Section 4. Finally, findings and future directions are summarised in Section 5.

2. Motivation: Clinical Problem

Missing values are a common challenge in healthcare datasets, arising from sources such as incomplete patient forms, survey non-responses [36], and technical glitches during data collection [57]. These missing values manifest within the data and affect study outcomes and statistical validity. Therefore, choosing appropriate methodological approaches to tackle this problem is crucial.

In critical care medicine, missing values are also a result of irregular and informative sampling [15]. To provide some context, clinicians in critical care monitor deviations from the expected arterial acidity (pH) range to gain insights into respiratory function, electrolyte balance, and the underlying diseases of the patients [46]. When pH deviates from normal ranges, either through acidosis ($\text{pH} < 7.3$) or alkalosis ($\text{pH} > 7.5$), it could disrupt vital biochemical processes and overall

equilibrium, with studies showing that blood pH levels are associated with the mortality rate [39, 22] and neurological recovery in cases of cardiopulmonary resuscitation [44].

One way to monitor and model the pH level is the Stewart-Fencel approach [48, 49, 12]. This approach identifies three independent variables that determine pH. The first variable is carbon dioxide (CO_2), a major source of acid in the body that can be continuously monitored using modern bedside equipment. The second and third variables are strong ion differences (e.g. Na^+ , K^+ , Cl^-) and weak acids (e.g. albumin, lactate, urea, phosphate), respectively. These components require blood tests for measurement, which are performed less frequently due to their invasive nature [3].

While CO_2 is also measured through capnography as a surrogate, known as end-tidal CO_2 (ETCO_2), the main interest is in blood CO_2 levels because they directly influence pH. In various respiratory conditions (such as asthma and COPD), the CO_2 in the blood does not equilibrate with CO_2 in the lungs. This creates a measurable gap between blood and alveolar CO_2 levels, which can also be informative [1, 27].

This disparity in measurement frequency creates a pattern of irregular sampling, where data collection occurs at inconsistent intervals. The resulting gaps in data collection lead to missing values, particularly for parameters requiring blood tests, as illustrated in Fig. 1. Consequently, the irregular nature of these measurements complicates the application of standard statistical techniques to analyse and interpret the data.

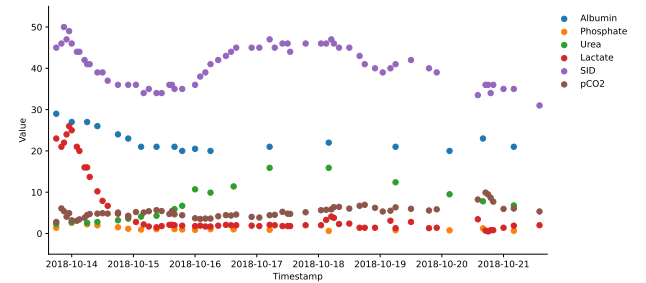


Fig. 1. Irregular sampling of six measurements of a sample patient. The pCO_2 , strong ion differences (SID), and lactate are measured from bedside monitoring, while albumin, phosphate, and urea levels are obtained from blood tests.

On the other hand, informative sampling occurs when data point selection is influenced by factors related to clinical hypotheses. For instance, clinicians might refrain from collecting data when a patient's health improves and vice versa [9]. In this context, both irregular and informative sampling scenarios fall under the Missing Not at Random (MNAR) category, as the missingness is not random but associated with unobserved data or specific conditions and the missingness carries information [31].

This study addresses the challenge of missing values in critical care data, which can impact patient outcome predictions [53], for example, in predicting in-hospital and 30-day mortality [43]. Rather than relying on complete-case analysis, which risks losing valuable information, this work proposes using deep GPs for data imputation. This approach leverages both cross-sectional and longitudinal information from patient records.

Following the Stewart-Fencel approach, the analysis is structured with arterial pH as the dependent variable.

Relevant covariates are constructed to identify factors causing pH deviations. The proposed method not only imputes missing values in the covariates but also quantifies the uncertainty associated with these imputations, providing a more comprehensive understanding of the data's reliability.

While this study focuses on its application in critical care medicine because of its clinical importance, the proposed method applies to different scenarios with similar conditions. For example, missing values are also found in human activity recognition from multiple sensor streams [19], sleep disorder diagnoses using electroencephalogram (EEG) [28], and hepatocellular carcinoma [16].

3. Methodology

3.1. Gaussian Processes

Let $\mathbf{X} \in \mathbb{R}^{N \times D}$ represent a D -dimensional input with N observed data points and $\mathbf{Y} \in \mathbb{R}^N$ be the corresponding outputs. Then, the GP model assumes that \mathbf{Y} follows a multivariate Gaussian distribution $\mathbf{Y} \sim \mathcal{N}(\boldsymbol{\mu}, \sigma^2 \mathbf{R}(\mathbf{X}))$, where $\boldsymbol{\mu} \in \mathbb{R}^N$ is the mean vector, σ^2 is the scale parameter, and $\mathbf{R}(\mathbf{X}) \in \mathbb{R}^{N \times N}$ is the correlation matrix. Cell ij in the matrix $\mathbf{R}(\mathbf{X})$ is specified by $k(\mathbf{X}_{i*}, \mathbf{X}_{j*}) + \eta \mathbb{1}_{\{\mathbf{X}_{i*} = \mathbf{X}_{j*}\}}$, where $k(\cdot, \cdot)$ is a given kernel function with η being the nugget term and $\mathbb{1}_{\{\cdot\}}$ being the indicator function. In this study, we consider Gaussian processes with zero means, i.e. $\boldsymbol{\mu} = \mathbf{0}$ and kernel functions with the multiplicative form: $k(\mathbf{X}_{i*}, \mathbf{X}_{j*}) = \prod_{d=1}^D k_d(X_{id}, X_{jd})$ where $k_d(X_{id}, X_{jd}) = k_d(|X_{id} - X_{jd}|)$ is a one-dimensional stationary and isotropic kernel function, e.g., squared exponential kernel function [38], for the d -th input dimension.

The hyperparameters σ^2 , η , and those contained in $k(\cdot, \cdot)$ are typically estimated using maximum likelihood or maximum a posteriori [38]. Given estimated GP hyperparameters, the realisations of input $\mathbf{x} = (\mathbf{x}_{1*}^T, \dots, \mathbf{x}_{N*}^T)^T$, and output $\mathbf{y} = (y_1, \dots, y_N)^T$, then the posterior predictive distribution of output Y_0 at a new input position $\mathbf{x}_0 \in \mathbb{R}^{1 \times D}$ follows a Gaussian distribution with mean μ_0 and variance σ_0^2 given by:

$$\mu_0 = \mathbf{r}(\mathbf{x}_0)^T \mathbf{R}(\mathbf{x})^{-1} \mathbf{y} \quad (1)$$

$$\sigma_0^2 = \sigma^2 (1 + \eta - \mathbf{r}(\mathbf{x}_0)^T \mathbf{R}(\mathbf{x})^{-1} \mathbf{r}(\mathbf{x}_0)) \quad (2)$$

where $\mathbf{r}(\mathbf{x}_0) = [k(\mathbf{x}_0, \mathbf{x}_{1*}), \dots, k(\mathbf{x}_0, \mathbf{x}_{N*})]^T$.

A GP model can be used as a smoothing function for irregularly sampled signals through the predicted mean function of a time series. Thus, GPs have been used to model electronic health records [26], wearable sensor data for e-health [10], gene expression data [13, 24, 32], and quantitative traits [52, 2].

3.2. Linked Gaussian Processes

Consider a GP model with N sets of D -dimensional input ($\mathbf{X} \in \mathbb{R}^{N \times D}$) and produces N sets of P -dimensional output ($\mathbf{W} \in \mathbb{R}^{N \times P}$). We can assume that the output \mathbf{W} of this model, i.e. the column vectors \mathbf{W}_{*p} , is conditionally independent with respect to \mathbf{X} . A linked GP (LGP) is then created when we link the output \mathbf{W} to a second GP model that produces N one-dimensional outputs ($\mathbf{Y} \in \mathbb{R}^N$). Let the GP surrogates of the two models be \mathcal{GP}_1 and \mathcal{GP}_2 , respectively. Then, \mathcal{GP}_1 is a collection of independent GPs, $\{\mathcal{GP}_1^{(p)}\}_{p=1, \dots, P}$, and the hierarchy of GPs that represents the system can be seen as in Fig. 2. As described in Subsection 3.1, we can see that each GP

corresponds to a multivariate Gaussian distribution with input \mathbf{X} and output \mathbf{W}_{*p} .

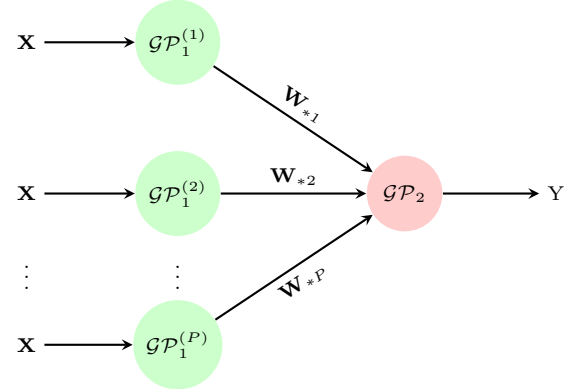


Fig. 2. A two-layered deep Gaussian process model

Assume that the model parameters involved in \mathcal{GP}_1 and \mathcal{GP}_2 are known or estimated and we observe realisations \mathbf{w} and \mathbf{y} of \mathbf{W} and \mathbf{Y} given inputs $\mathbf{X} = \mathbf{x}$. Then, the posterior predictive distribution of the global output Y_0 at a new global input position \mathbf{x}_0 is given by $Y_0|\mathcal{D} \sim p(y_0|\mathbf{x}_0; \mathbf{y}, \mathbf{w}, \mathbf{x})$, where $\mathcal{D} = \{\mathbf{Y} = \mathbf{y}, \mathbf{W} = \mathbf{w}, \mathbf{X} = \mathbf{x}\}$ and $p(y_0|\mathbf{y}, \mathbf{w}, \mathbf{x})$ is the PDF of $Y_0|\mathcal{D}$. Note that

$$\begin{aligned} p(y_0|\mathbf{x}_0; \mathbf{y}, \mathbf{w}, \mathbf{x}) &= \int p(y_0|\mathbf{w}_0; \mathbf{y}, \mathbf{w}, \mathbf{x}) p(\mathbf{w}_0|\mathbf{x}_0; \mathbf{y}, \mathbf{w}, \mathbf{x}) d\mathbf{w}_0 \\ &= \int p(y_0|\mathbf{w}_0; \mathbf{y}, \mathbf{w}) \prod_{p=1}^P p(w_{0p}|\mathbf{x}_0; \mathbf{w}_{*p}^*, \mathbf{x}) d\mathbf{w}_0 \end{aligned} \quad (3)$$

where $p(y_0|\mathbf{w}_0; \mathbf{y}, \mathbf{w})$ and $p(w_{0p}|\mathbf{x}_0; \mathbf{w}_{*p}^*, \mathbf{x})$ are PDF's of the posterior predictive distributions of GP_2 and $GP_1^{(p)}$, respectively; and $\mathbf{w}_0 = (w_{01}, \dots, w_{0P})$. However, $p(y_0|\mathbf{x}_0; \mathbf{y}, \mathbf{w}, \mathbf{x})$ is analytically intractable because the integral in Equation 3 does not have a closed form expression. It can be shown that, given the GP specifications in Subsection 3.1, the mean, $\tilde{\mu}_0$, and variance, $\tilde{\sigma}_0^2$, of $Y_0|\mathcal{D}$ are expressed analytically as follows:

$$\tilde{\mu}_0 = \mathbf{I}(\mathbf{x}_0)^T \mathbf{R}(\mathbf{w})^{-1} \mathbf{y} \quad (4)$$

$$\begin{aligned} \tilde{\sigma}_0^2 &= \mathbf{y}^T \mathbf{R}(\mathbf{w})^{-1} \mathbf{J}(\mathbf{x}_0) \mathbf{R}(\mathbf{w})^{-1} \mathbf{y} - \left[\mathbf{I}(\mathbf{x}_0)^T \mathbf{R}(\mathbf{w})^{-1} \mathbf{y} \right]^2 \\ &\quad + \sigma^2 \left(1 + \eta - \text{tr} \left[\mathbf{R}(\mathbf{w})^{-1} \mathbf{J}(\mathbf{x}_0) \right] \right) \end{aligned} \quad (5)$$

where $\mathbf{I}(\mathbf{x}_0) \in \mathbb{R}^{N \times 1}$ with its i th element $I_i = \prod_{p=1}^P \mathbb{E}[k_p(W_{0p}(\mathbf{x}_0), w_{ip})]$; $\mathbf{J}(\mathbf{x}_0) \in \mathbb{R}^{N \times N}$ with its ij th element $J_{ij} = \prod_{p=1}^P \mathbb{E}[k_p(W_{0p}(\mathbf{x}_0), w_{ip}) k_p(W_{0p}(\mathbf{x}_0), w_{jp})]$; and the expectations in $\mathbf{I}(\mathbf{x}_0)$ and $\mathbf{J}(\mathbf{x}_0)$ have closed-form expressions under the linear kernel, squared exponential kernel, and a class of Matérn kernels [50, 25, 33]. The linked GP is then defined as a Gaussian approximation $\hat{p}(y_0|\mathbf{x}_0; \mathbf{y}, \mathbf{w}, \mathbf{x})$ with its mean and variance given by $\tilde{\mu}_0$ and $\tilde{\sigma}_0^2$. Furthermore, the linked GP can be built iteratively to analytically approximate the posterior predictive distribution of outputs from any feed-forward GP systems. Research has shown that this approach provides an adequate approximation by minimising the Kullback-Leibler divergence [33].

3.3. Deep Gaussian Processes

A deep GP (DGP) model can be seen as a linked GP model when the internal inputs/outputs of GPs are latent. Thus, Fig. 2 can be seen as a two-layered deep GP with unobserved values of variable \mathbf{W} . The latent variables make conducting efficient inference for deep GP models harder. For instance, to train the two-layer deep GP by the maximum likelihood approach, one needs to optimise the model parameters by maximising the likelihood function:

$$\mathcal{L} = p(\mathbf{y}|\mathbf{x}) = \int p(\mathbf{y}|\mathbf{w}) \prod_{p=1}^P p(\mathbf{w}_{*p}|\mathbf{x}) d\mathbf{w}, \quad (6)$$

where $p(\mathbf{y}|\mathbf{w})$ is the multivariate Gaussian PDF of \mathcal{GP}_2 and $p(\mathbf{w}_{*p}|\mathbf{x})$ is the multivariate Gaussian PDF of $\mathcal{GP}_1^{(p)}$. However, due to the nonlinearity between \mathbf{y} and \mathbf{w} , the integral with respect to the latent variable \mathbf{w} in Equation 6 is analytically intractable. As we increase the depth of a deep GP, the number of such intractable integrals will also increase.

3.4. Deep GP with Stochastic Imputation

Recently, stochastic imputation (SI) was proposed to tackle the inference issue in deep GP [34], leveraging the fact that DGP and LGP are similar in structure. This approach provides a well-balanced trade-off between computational complexity and accuracy by combining the computational efficiency of variational inference [41] and the accuracy of a full Bayesian approach [42]. The key concept of SI is converting a DGP emulator to multiple LGP emulators, each representing a DGP realisation with imputed latent variables.

Given a similar DGP emulator hierarchy as described in Subsection 3.2 (Fig. 2) and realisations \mathbf{y} of \mathbf{Y} , we can obtain point estimates of unknown model parameters in $\mathcal{GP}_1^{(p)}$ for all $p = 1, \dots, P$ and \mathcal{GP}_2 , using the Stochastic Expectation Maximization (SEM) algorithm [34]. With the estimated model parameters, the DGP emulator gives the approximate posterior predictive mean and variance of $y_0(\mathbf{x}_0)$ at a new input position \mathbf{x}_0 as described in Algorithm 1.

Algorithm 1 Construction of a DGP emulator with the hierarchy in Figure 2

Input: i) Realisations \mathbf{x} and \mathbf{y} ; ii) A new input position \mathbf{x}_0 ; iii) The number of imputations N .

Output: Mean and variance of $y_0(\mathbf{x}_0)$.

- 1: **for** $i = 1, \dots, N$ **do**
- 2: Given \mathbf{x} and \mathbf{y} , draw an imputation $\{\mathbf{w}_{*p,i}\}_{p=1,\dots,P}$ of the latent output $\{\mathbf{W}_{*p}\}_{p=1,\dots,P}$ via an Elliptical Slice Sampling [35] update.
- 3: Construct the LGP emulator \mathcal{LGP}_i with the mean $\tilde{\mu}_{0,i}(\mathbf{x}_0)$ and variance $\tilde{\sigma}_{0,i}^2(\mathbf{x}_0)$, given \mathbf{x} , \mathbf{y} , and $\{\mathbf{w}_{*p,i}\}$.
- 4: **end for**
- 5: Compute the mean $\mu(\mathbf{x}_0)$ and variance $\sigma^2(\mathbf{x}_0)$ of $y_0(\mathbf{x}_0)$ by

$$\mu(\mathbf{x}_0) = \frac{1}{N} \sum_{i=1}^N \tilde{\mu}_{0,i}(\mathbf{x}_0),$$

$$\sigma^2(\mathbf{x}_0) = \frac{1}{N} \sum_{i=1}^N \left([\tilde{\mu}_{0,i}(\mathbf{x}_0)]^2 + \tilde{\sigma}_{0,i}^2(\mathbf{x}_0) \right) - \mu(\mathbf{x}_0)^2.$$

One can extend Algorithm 1 to multiple layers $l = 1, \dots, L$ and multiple outputs $\mathbf{y}_0(\mathbf{x}_0)$ by applying the same algorithm

and repeating step 2 for each layer. A detailed explanation of this generalisation is provided in [34].

3.5. Benchmarking

Our numerical experiments evaluated five different models to analyse the dataset.

Linked GP with sequential design

This hierarchical approach consisted of three steps. First, we fitted individual GPs for each covariate using timestamps and removing observations with missing values (i.e. complete case analysis). Second, we trained a GP to predict the output variable using these covariates. Finally, we connected these GPs into a hierarchical structure, allowing output variable prediction even when covariate data is missing.

Deep GP with stochastic imputation

In contrast to the separated training approach, we trained a unified deep GP model that integrated all components: it took timestamp as input, processed covariates in the latent layer, and predicted the output variable as output—all within a single end-to-end framework as described in Subsection 3.4.

To set the baseline for our proposed models, we compared them with the following approaches:

1. Last-known value imputation: we used the last-known value of the variable until the next measurement is observed [45];
2. MICE: multiple imputation using chained equations [20]—ignoring the temporal dependency, relying only on the cross-sectional information between variables by treating each observation as independent and identically distributed [40, 31], and doing iterative imputation;
3. GP interpolation: we fitted a GP regressor with a squared exponential kernel individually for each covariate and the output variable.

4. Numerical Experiments

4.1. Clinical Problem

Building on the Stewart-Fencel approach, the model was constructed with pH as the dependent variable and three independent variables: CO₂ levels, strong ion differences (SID), and weak acid concentrations. As such, two experiments were conducted in this study:

1. Development of a continuous pH estimation model based on the Stewart-Fencel approach [49].
2. Simulation of real-world clinical scenarios by deliberately masking (intentionally withholding) portions of the covariates, mirroring the practical challenges of aligning laboratory test results with continuous bedside monitoring. Using measured pH levels to impute these missing covariate values, the aim was to provide clinicians with insights into patient status between laboratory tests.

The experiments were done on a dataset of 14 ICU admission windows selected at random from a paediatric intensive care unit. Each admission had a different number of data points, ranging from 19 to 115 hourly timestamps, and some patients had multiple admissions. To further de-identify the patients, the dates were shifted to future dates while retaining the time relationships.

To follow the physicochemical approach of acid-base balance, the model incorporated multiple blood gas measurements.

Specifically, the model used partial carbon dioxide pressure ($p\text{CO}_2$) and pH measurements and the difference between Na^+ and Cl^- concentrations to represent the SID [23]. Although CO_2 levels can be measured through both blood gas analysis [17] and capnography (ETCO_2) [37], the numerical experiment was simplified by using only blood gas measurements. For acid-base balance modelling, blood gas measurements are generally preferred over capnography for CO_2 because they offer a more comprehensive and direct assessment of the body's acid-base status [1, 27]. Additionally, due to limited observations in half of the admission windows, the weak acid component was represented by lactate measurements from the blood gas analyser.

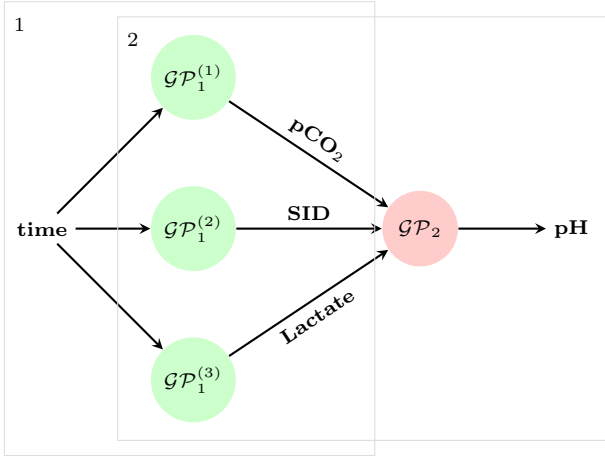


Fig. 3. A two-layered deep Gaussian process (DGP) for pH prediction. This study compares two fitting approaches: the linked GP with sequential design (LGP), which fits the layers separately (first predicting the covariates, then pH) and the DGP with stochastic imputation (SI) method, where all the components are trained simultaneously.

The DGP-SI model was trained simultaneously for all components using the architecture illustrated in Fig. 3. For comparison, an ablation study was also conducted using an LGP model with a sequential design. This linked model operates in two steps: (1) it used separate GPs to predict three covariates ($p\text{CO}_2$, SID, and lactate) from time inputs; (2) it combined these predicted covariates to forecast pH. For a fair comparison, the MICE model only used time and pH data, excluding covariates since these would not be available during the inference process of our proposed models.

Following the literature, the data was preprocessed through several steps. First, the data was discretised into sequences of hourly intervals and aggregated the measurements by taking the arithmetic means [30, 14]. Then, to evaluate the model's robustness, either the observed pH or the covariates were randomly masked with varying proportions (10%, 20%, 30%, and 40%) [18, 5]. Finally, z-score transformation was applied to both pH values and the covariates to standardise the data distribution.

To evaluate model performance given the presence of measurement noise, the accuracy of missing value imputations was defined as the mean absolute error (MAE):

$$MAE = \frac{1}{N \times D} \sum_{i=1}^N \sum_{d \in D} |X_{id} - \hat{X}_{id}| \quad (7)$$

where N is the total number of missing values being evaluated, X_{id} is the i -th true value that was masked and \hat{X}_{id} is the i -th estimated value at dimension d . In the GP-based methods, the model prediction is computed as the mean of the predictive distribution.

4.2. Results

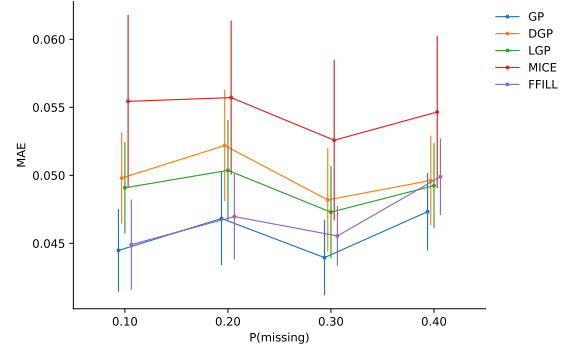


Fig. 4. Average MAE values in predicting pH values. The error bar represents the standard error of the MAE values across all admission windows.

Predicting pH values

To ensure comparable results, all models were standardised to use time as the input variable and pH as the target variable. While predicting pH values, the model only used time as the predictor variable and information from other covariates was excluded. Additionally, the last-known imputation method only used the most recent pH measurements, while in the single GP fitting, pH measurements before and after the missing data points were interpolated. Although the DGP and LGP models had access to covariate information as the latent variables during their development, they also operated with time as their only input variable during the inference process.

The analysis of prediction errors revealed a hierarchy among the imputation methods of pH values. As shown in Fig. 4, the GP interpolation outperformed other methods, maintaining the lowest error rates even as the proportion of missing values increased. Following closely, the last-known imputation method had comparable average errors to the GP interpolation when the proportion of missingness is 10% or 20%, but showed declining accuracy at higher proportions. DGP and LGP models ranked in the middle, performing better than MICE but worse than both GP interpolation and last-known imputation. Their reduced accuracy might stem from uncertainty propagation through their latent variables. MICE, which ignores temporal relationships by treating timesteps independently, consistently showed the highest error rates.

Imputing missing values in covariates

Unlike the pH value prediction, where missing values were filled out from a single variable, the second experiment predicted missing values with varying proportions from three variables: $p\text{CO}_2$, SID, and lactate as the weak acid. All three variables were measured at the same time as pH. This experiment used all the observed pH values to link the three covariates as suggested by the Stewart-Fencl physicochemical approach. Since the linked GP, in this case, was just individually fitted

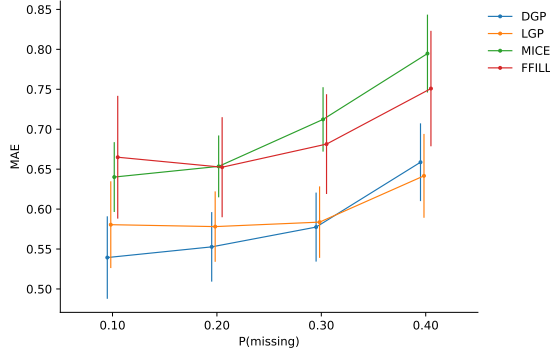


Fig. 5. Average MAE values in imputing the covariates. The error bar represents the standard error of the MAE values across all admission windows. DGP, which combines longitudinal and cross-sectional information, performs better in imputing missing values in the covariates, particularly at lower missingness levels. However, as the proportion of missing values increases, methods that rely on longitudinal information become more effective.

GPs with complete case analysis, there were only four models to compare in this experiment.

The performance comparison revealed that DGP achieved the lowest error rates at 10% and 20% missing values, performed similarly to LGP at 30%, and slightly underperformed compared to LGP at 40% (Figure 5). Both DGP and LGP demonstrated better performance than MICE and last-known imputation methods, with last-known imputation showing lower error rates than MICE as missingness increased. These findings suggest that longitudinal information is more valuable than cross-sectional information for covariate imputation. However, DGP’s low error rates indicate that combining both longitudinal and cross-sectional information yields optimal results.

Uncertainty quantification

As the covariates were connected through pH in the output layer using DGP-SI, an observation from one covariate could affect the uncertainty of another covariate when an observation was unavailable. To demonstrate this effect, differences in uncertainty were compared by manually masking observations from the three covariates in three different intervals, focusing on masking lactate within these intervals. The experiment revealed that the uncertainty in lactate, shown in Fig. 6, was less when only the observed points in lactate were masked instead of all three covariates being masked.

5. Discussion

This paper demonstrated that DGP-SI, initially developed for uncertainty quantification in computationally expensive models, could effectively handle missing values in critical care data from different sources. The analysis across 14 admission windows showed that DGP-SI performed better in imputing missing covariate values, particularly when the proportion of missing data was low. This approach offers clinicians insight into patient states between measurements whilst providing uncertainty quantification, hence attaching a measure of confidence that addresses the inherent uncertainties in medical science [7].

From a clinical perspective, accurately imputing missing values with quantified uncertainty can impact decision-making,

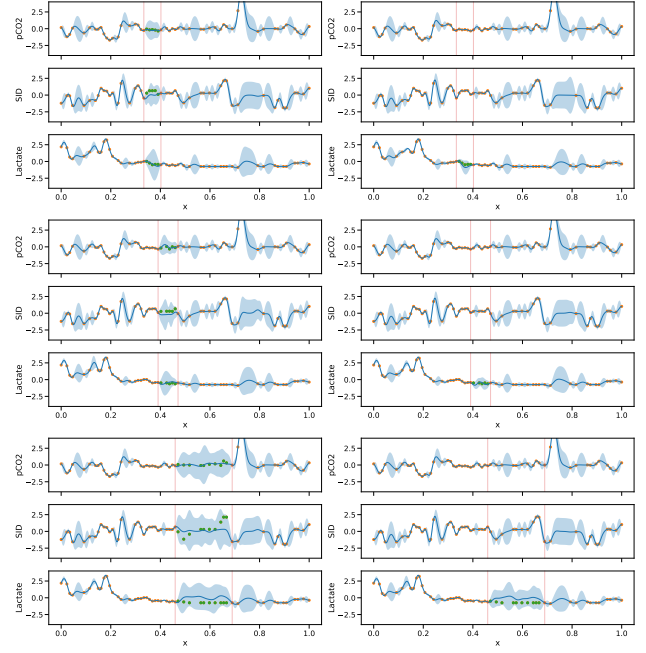


Fig. 6. Uncertainty quantification derived from the DGP-SI model when imputing missing values in the covariates. Orange dots represent observed values, while green dots (between red vertical lines) show masked values. The x-axis shows scaled time, and the y-axis shows standardised covariate values. The uncertainty for lactate resulting from manually masking the three covariates (left) is greater than that from only masking lactate (right).

especially in time-sensitive critical care scenarios. Clinicians often face the challenge of making treatment decisions with incomplete data, and the uncertainty quantification provided by DGP-SI could be valuable for retrospective analyses of acid-base disorders where multiple parameters interact in complex ways that clinicians find difficult to intuit. Additionally, this method has the potential to enhance early warning systems in intensive care units by providing more complete data streams for continuous patient monitoring, identifying deteriorating patients earlier while reducing false alarms.

The proposed approach also poses challenges for future work with two main limitations. First, it is less effective in emulating the Stewart-Fencl physicochemical model for pH prediction, likely due to error propagation through intermediate variables. Second, as highlighted in [34], the method becomes computationally expensive with larger datasets. To handle this, the data was partitioned into shorter admission windows. However, such an approach may not be feasible in settings with high-frequency measurements, such as those from wearable devices.

To address these limitations, several paths forward exist. The computational burden can be reduced through time discretisation and data aggregation, as demonstrated in this work. Alternative solutions include implementing sparse GP approximations [47, 4] or utilising GPU parallelisation for exact GP computations [54]. Additionally, further research should evaluate the model’s performance on multimodal datasets with naturally varying patterns of missing data, focusing on scenarios where sufficient observations exist to be emulated using a deep GP model.

6. Competing interests

No competing interest is declared.

7. Author contributions statement

A.A.S., D.M., and F.A.D. conceived the experiment(s), A.A.S. conducted the experiment(s), A.A.S., D.M., and F.A.D. analysed the results. A.A.S. wrote the original manuscript. D.M., F.A.D., T.J., and S.R. reviewed and edited the manuscript.

8. Acknowledgements

This work was supported by the UK Engineering and Physical Sciences Research Council [EP/W523835/1 to A.A.S.].

References

1. Cynthia T Anderson and Peter H Breen. Carbon dioxide kinetics and capnography during critical care. *Critical Care*, 4(4):207, 2000.
2. Arttu Arjas, Andreas Hauptmann, and Mikko J Sillanpää. Estimation of dynamic snp-heritability with bayesian gaussian process models. *Bioinformatics*, 36(12):3795–3802, March 2020.
3. Philip S Barie. Phlebotomy in the intensive care unit: strategies for blood conservation. *Critical Care*, 8(Suppl 2):S34, 2004.
4. Matthias Bauer, Mark Van der Wilk, and Carl Edward Rasmussen. Understanding probabilistic sparse gaussian process approximations. *Advances in neural information processing systems*, 29, 2016.
5. Brett K Beaulieu-Jones, Jason H Moore, and Pooled Resource Open-Access ALS Clinical Trials Consortium. Missing data imputation in the electronic health record using deeply learned autoencoders. In *Pacific symposium on biocomputing 2017*, pages 207–218. World Scientific, 2017.
6. Luca Biggio, Alexander Wieland, Manuel Arias Chao, Iason Kastanis, and Olga Fink. Uncertainty-aware prognosis via deep Gaussian process. *IEEE Access*, 9:123517–123527, 2021.
7. Federico Cabitza, Raffaele Rasoini, and Gian Franco Gensini. Unintended consequences of machine learning in medicine. *JAMA*, 318(6):517, August 2017.
8. Wei Cao, Dong Wang, Jian Li, Hao Zhou, Lei Li, and Yitan Li. BRITS: Bidirectional recurrent imputation for time series. In *Advances in neural information processing systems*, volume 31, 2018.
9. Zhengping Che, Sanjay Purushotham, Kyunghyun Cho, David Sontag, and Yan Liu. Recurrent neural networks for multivariate time series with missing values. *Scientific reports*, 8(1):6085, 2018.
10. Lei Clifton, David A Clifton, Marco AF Pimentel, Peter J Watkinson, and Lionel Tarassenko. Gaussian processes for personalized e-health monitoring with wearable sensors. *IEEE Transactions on Biomedical Engineering*, 60(1):193–197, 2012.
11. Andreas Damianou and Neil D Lawrence. Deep Gaussian processes. In *Proceedings of the Sixteenth International Conference on Artificial Intelligence and Statistics*, volume 31, pages 207–215. PMLR, 2013.
12. Vladimir Fencel and David E Leith. Stewart’s quantitative acid-base chemistry: applications in biology and medicine. *Respiration physiology*, 91(1):1–16, 1993.
13. Pei Gao, Antti Honkela, Magnus Rattray, and Neil D. Lawrence. Gaussian process modelling of latent chemical species: applications to inferring transcription factor activities. *Bioinformatics*, 24(16):i70–i75, August 2008.
14. Ghadeer O Ghosheh, Jin Li, and Tingting Zhu. IGnite: Individualized generation of imputations in time-series electronic health records. *arXiv preprint arXiv:2401.04402*, 2024.
15. Rolf H. H. Groenwold. Informative missingness in electronic health record systems: the curse of knowing. *Diagnostic and Prognostic Research*, 4(1):1–6, December 2020.
16. Seungbong Han, Kam-Wah Tsui, Hui Zhang, Gi-Ae Kim, Young-Suk Lim, and Adin-Cristian Andrei. Multiple imputation analysis for propensity score matching with missing causes of failure: An application to hepatocellular carcinoma data. *Statistical Methods in Medical Research*, 30(10):2313–2328, September 2021.
17. Wael Hassan and Seth Martinez. Arterial blood gas sampling [ABG machine use]. In *StatPearls [Internet]*. StatPearls Publishing, 2024.
18. Bahram Jafrasteh, Daniel Hernández-Lobato, Simón Pedro Lubián-López, and Isabel Benavente-Fernández. Gaussian processes for missing value imputation. *Knowledge-Based Systems*, 273:110603, August 2023.
19. Yash Jain, Chi Ian Tang, Chulhong Min, Fahim Kawsar, and Akhil Mathur. ColloSSL: Collaborative self-supervised learning for human activity recognition. *Proceedings of the ACM on Interactive, Mobile, Wearable and Ubiquitous Technologies*, 6(1):1–28, 2022.
20. Daniel Jarrett, Bogdan Cebere, Tennison Liu, Alicia Curth, and Mihaela van der Schaar. Hyperimpute: Generalized iterative imputation with automatic model selection. 2022.
21. Alistair E.W. Johnson, Tom J. Pollard, Lu Shen, Li-wei H. Lehman, Mengling Feng, Mohammad Ghassemi, Benjamin Moody, Peter Szolovits, Leo Anthony Celi, and Roger G. Mark. MIMIC-III, a freely accessible critical care database. *Scientific Data*, 3(1), May 2016.
22. Boris Jung, Thomas Rimmel, Charlotte Le Goff, Gérald Chanques, Philippe Corne, Olivier Jonquet, Laurent Muller, Jean-Yves Lefrant, Christophe Guervilly, Laurent Papazian, Bernard Allaouchiche, and Samir Jaber. Severe metabolic or mixed acidemia on intensive care unit admission: incidence, prognosis and administration of buffer therapy. a prospective, multiple-center study. *Critical Care*, 15(5), October 2011.
23. John A Kellum. Determinants of blood pH in health and disease. *Critical Care*, 4(1):6, 2000.
24. Paul D. W. Kirk and Michael P. H. Stumpf. Gaussian process regression bootstrapping: exploring the effects of uncertainty in time course data. *Bioinformatics*, 25(10):1300–1306, March 2009.
25. Ksenia N Kyzurova, James O Berger, and Robert L Wolpert. Coupling computer models through linking their statistical emulators. *SIAM/ASA Journal on Uncertainty Quantification*, 6(3):1151–1171, 2018.
26. Thomas A. Lasko, Joshua C. Denny, and Mia A. Levy. Computational phenotype discovery using unsupervised feature learning over noisy, sparse, and irregular clinical data. *PLoS ONE*, 8(6):e66341, June 2013.
27. Daniel H. Lee, Brian E. Driver, and Robert F. Reardon. Pitfalls of overreliance on capnography and disregard of

- visual evidence of tracheal tube placement: A pediatric case series. *JEM Reports*, 3(1):100061, March 2024.
28. Woonghee Lee, Jaeyoung Lee, and Younghoon Kim. Contextual imputation with missing sequence of EEG signals using generative adversarial networks. *IEEE Access*, 9:151753–151765, 2021.
 29. Yikuan Li, Shishir Rao, Abdelaali Hassaine, Rema Ramakrishnan, Dexter Canoy, Gholamreza Salimi-Khorshidi, Mohammad Mamouei, Thomas Lukasiewicz, and Kazem Rahimi. Deep Bayesian Gaussian processes for uncertainty estimation in electronic health records. *Scientific reports*, 11(1):20685, 2021.
 30. Zachary C Lipton, David Kale, and Randall Wetzel. Directly modeling missing data in sequences with RNNs: Improved classification of clinical time series. In Finale Doshi-Velez, Jim Fackler, David Kale, Byron Wallace, and Jenna Wiens, editors, *Proceedings of the 1st Machine Learning for Healthcare Conference*, volume 56 of *Proceedings of Machine Learning Research*, pages 253–270, Northeastern University, Boston, MA, USA, 18–19 Aug 2016. PMLR.
 31. Roderick JA Little and Donald B Rubin. *Statistical analysis with missing data*, volume 793. John Wiley & Sons, 2019.
 32. Qiang Liu, Kevin K. Lin, Bogi Andersen, Padhraic Smyth, and Alexander Ihler. Estimating replicate time shifts using gaussian process regression. *Bioinformatics*, 26(6):770–776, February 2010.
 33. Deyu Ming and Serge Guillas. Linked Gaussian process emulation for systems of computer models using Matérn kernels and adaptive design. *SIAM/ASA Journal on Uncertainty Quantification*, 9(4):1615–1642, 2021.
 34. Deyu Ming, Daniel Williamson, and Serge Guillas. Deep Gaussian process emulation using stochastic imputation. *Technometrics*, 65(2):150–161, 2023.
 35. Robert Nishihara, Iain Murray, and Ryan P Adams. Parallel MCMC with generalized elliptical slice sampling. *The Journal of Machine Learning Research*, 15(1):2087–2112, 2014.
 36. Kay I Penny and Ian Atkinson. Approaches for dealing with missing data in health care studies. *Journal of clinical nursing*, 21(19pt20):2722–2729, 2012.
 37. Marc R Raffe. Oximetry and capnography. In *The Veterinary ICU Book*, pages 86–95. CRC Press, 2020.
 38. Carl Edward Rasmussen and Christopher K. I. Williams. *Gaussian Processes for Machine Learning*. The MIT Press, 2006.
 39. S Rodríguez-Villar, JA Kraut, J Arévalo-Serrano, SG Sakka, C Harris, I Awad, M Toolan, S Vanapalli, A Collins, A Spataru, P Eiben, V Recea, C Brathwaite-Shirley, L Thompson, B Gurung, and R Reece-Anthony. Systemic acidemia impairs cardiac function in critically ill patients. *eClinicalMedicine*, 37:100956, July 2021.
 40. Donald B. Rubin. *Multiple Imputation for Nonresponse in Surveys*. Wiley, June 1987.
 41. Hugh Salimbeni and Marc Deisenroth. Doubly stochastic variational inference for deep gaussian processes. *Advances in neural information processing systems*, 30, 2017.
 42. Annie Sauer, Robert B. Gramacy, and David Higdon. Active learning for deep Gaussian process surrogates. *Technometrics*, 65(1):4–18, February 2022.
 43. Anis Sharafoddini, Joel A Dubin, David M Maslove, and Joon Lee. A new insight into missing data in intensive care unit patient profiles: Observational study. *JMIR Medical Informatics*, 7(1):e11605, January 2019.
 44. Jonghwan Shin, Yong Su Lim, Kyuseok Kim, Hui Jai Lee, Se Jong Lee, Euigi Jung, Kyoung Min You, Hyuk Jun Yang, Jin Joo Kim, Joonghee Kim, You Hwan Jo, Jae Hyuk Lee, and Seong Youn Hwang. Initial blood pH during cardiopulmonary resuscitation in out-of-hospital cardiac arrest patients: a multicenter observational registry-based study. *Critical Care*, 21(1), December 2017.
 45. Ohidul Siddiqui and Mirza W. Ali. A comparison of the random-effects pattern mixture model with last-observation-carried-forward (LOCF) analysis in longitudinal clinical trials with dropouts. *Journal of Biopharmaceutical Statistics*, 8(4):545–563, January 1998.
 46. AA Sirker, A Rhodes, RM Grounds, and ED Bennett. Acid-base physiology: the ‘traditional’ and the ‘modern’ approaches. *Anaesthesia*, 57(4):348–356, 2002.
 47. Edward Snelson and Zoubin Ghahramani. Local and global sparse gaussian process approximations. In *Artificial Intelligence and Statistics*, pages 524–531. PMLR, 2007.
 48. Peter A. Stewart. Independent and dependent variables of acid-base control. *Respiration Physiology*, 33(1):9–26, April 1978.
 49. Peter A Stewart. Modern quantitative acid–base chemistry. *Canadian journal of physiology and pharmacology*, 61(12):1444–1461, 1983.
 50. Michalis Titsias and Neil D Lawrence. Bayesian gaussian process latent variable model. In *Proceedings of the thirteenth international conference on artificial intelligence and statistics*, pages 844–851. JMLR Workshop and Conference Proceedings, 2010.
 51. Antonia Tsvetanova, Matthew Sperrin, Niels Peek, Iain Buchan, Stephanie Hyland, and Glen P. Martin. Missing data was handled inconsistently in UK prediction models: a review of method used. *Journal of Clinical Epidemiology*, 140:149–158, December 2021.
 52. Jarno Vanhatalo, Zitong Li, and Mikko J Sillanpää. A gaussian process model and bayesian variable selection for mapping function-valued quantitative traits with incomplete phenotypic data. *Bioinformatics*, 35(19):3684–3692, March 2019.
 53. Aurélien Vesin, Elie Azoulay, Stéphane Ruckly, Lucile Vignoud, Kateřina Rusinová, Dominique Benoit, Marcio Soares, Paulo Azevedo-Maia, Fekri Abroug, Judith Benbenishty, and Jean Francois Timsit. Reporting and handling missing values in clinical studies in intensive care units. *Intensive Care Medicine*, 39(8):1396–1404, May 2013.
 54. Ke Wang, Geoff Pleiss, Jacob Gardner, Stephen Tyree, Kilian Q Weinberger, and Andrew Gordon Wilson. Exact gaussian processes on a million data points. *Advances in neural information processing systems*, 32, 2019.
 55. A Yarkın Yıldız, Emirhan Koç, and Aykut Koç. Multivariate time series imputation with transformers. *IEEE Signal Processing Letters*, 29:2517–2521, 2022.
 56. Jiaxuan You, Xiaocheng Li, Melvin Low, David Lobell, and Stefano Ermon. Deep Gaussian process for crop yield prediction based on remote sensing data. In *Proceedings of the AAAI conference on artificial intelligence*, volume 31, 2017.
 57. Yili Zhang and Güneş Koru. Understanding and detecting defects in healthcare administration data: Toward higher data quality to better support healthcare operations and decisions. *Journal of the American Medical Informatics Association*, 27(3):386–395, December 2019.